Dynamics driven by lipophilic force in Langmuir monolayers: In-plane and out-of-plane growth

Uttam Kumar Basak* and Alokmay Datta†

Surface Physics and Material Science Division, Saha Institute of Nuclear Physics, 1/AF Bidhannagar, Kolkata-700064, India

(Received 21 October 2014; revised manuscript received 12 February 2015; published 22 April 2015)

While monolayer area fraction versus time (A_n-t) curves obtained from surface pressure–area (π-A) isotherms for desorption-dominated (DD) processes in Langmuir monolayers of fatty acids represent continuous loss, those from Brewster angle microscopy (BAM) also show a two-dimensional (2D) coalescence. For nucleation-dominated (ND) processes both techniques suggest competing processes, with BAM showing 2D coalescence alongside multilayer formation. π enhances both DD and ND processes with a lower cutoff for ND processes, while temperature has a lower cutoff for DD but negligible effect on ND processes. Hydrocarbon chain length has the strongest effect, causing a crossover from DD to ND dynamics. Imaging ellipsometry of horizontally transferred films onto Si(100) shows Stranski-Krastanov-like growth for ND process in an arachidic acid monolayer resulting in successive stages of monolayer, trilayer, and multilayer islands, ridges from lateral island coalescence, and shallow wavelike structures from ridge coalescence on the film surface. These studies show that lipophilic attraction between hydrocarbon chains is the driving force at all stages of long-term monolayer dynamics.

DOI: 10.1103/PhysRevE.91.042405 PACS number(s): 68.18.Jk, 68.37.−d, 07.60.Fs

I. INTRODUCTION

Langmuir monolayers (LMs) composed of amphiphilic molecules have a wide range of applications especially in mimicking biological membranes and in growing Langmuir-Blodgett (LB) multilayers of tunable thickness and packing density [1–9] with applications in, for example, electrical, electronic, and optical device fabrication [10–15]. Stability of LMs is essential for studying their physicochemical properties as well as ensuring the perfection and thus the reproducibility of the LB multilayers grown from the LMs. Langmuir monolayers are at various levels of metastability above the equilibrium spreading pressure, i.e., the surface pressure [$\pi = \gamma - \gamma_0$, $\gamma_0(\gamma)$ being the surface tension of pure (monolayer-covered) water] spontaneously generated when the bulk amphiphile is brought into contact with a water surface [16,17], and they destabilize through the two-dimensional (2D) to three-dimensional (3D) transition, turning into bilayers or multilayers. When these multilayers grow in air the process is called "nucleation" [18] while the movement of molecules from the monolayer to water is called "desorption" [19,20]. Both processes are irreversible for single-tailed amphiphiles.

In this system there are three short-range molecular forces—the hydrophilic attraction between head groups of amphiphilic molecules and water, the hydrophobic repulsion between the tails and water, and the lipophilic attraction between the tails of adjacent molecules. During the formation of monolayers the competition between the first two forces plays the key role while the importance of the third grows as the surface density is increased, as is expected. Growth of Langmuir monolayers of fatty acids with the emergence of different structural phases at different surface concentrations or surface pressures has been thoroughly studied [21], as has been the dynamics at very high π values, i.e., collapse [22–27]. However, even basic questions regarding the long-term dynamics of Langmuir monolayers at lower surface pressure in the purported "stable" zones, such as the specific differences in dynamics of monolayers that destabilize through a desorption-dominated (DD) mechanism from those undergoing a nucleation-dominated (ND) destabilization have not been addressed, and the major destabilizing force among the above three has not been identified. This is essential in order to understand and control the process of destabilization and requires (a) long-term study of the dynamics of monolayer under the DD and ND processes, i.e., with amphiphiles having different tail lengths, (b) combination of probes at different length scales, and (c) probing the dynamics through field parameters like π and temperature.

In this paper, the long-term in-plane dynamics in Langmuir monolayers of single-tailed amphiphilic fatty acids at different temperatures and surface pressures away from collapse pressure is studied macroscopically through surface pressure–specific molecular area (π-A) isotherms and mesoscopically through Brewster angle microscopy (BAM). We have considered the tail length of the amphiphilic fatty acid molecule to be an "internal" parameter for the destabilization dynamics and have studied its effect through data on a series of amphiphilic fatty acids with tail lengths varying from 14 to 20 carbon atoms. We have also studied the out-of-plane dynamics of a long-chain fatty acid through imaging ellipsometry (IE).

II. EXPERIMENTAL DETAILS

The amphiphilic fatty acids myristic acid (C14), palmitic acid (C16), stearic acid (C18), and arachidic acid (C20), containing the same polar carboxylic (COOH) head group but 14, 16, 18, and 20 carbon atoms in their tails, respectively, with quoted purity >99% (Sigma-Aldrich) were dissolved in chloroform (Merck) to prepare 3 mM solutions, spread in a Langmuir trough (KSV NIMA, Biolin Scientific) on Milli-Q water (resistivity 18.2 MΩ cm) at room temperature (25 °C) and compressed with a speed of 5 cm^2/min after solvent evaporation and equilibration.

Surface pressure was measured by a paper Wilhelmy plate. Relaxation curves were obtained by recording the monolayer area with time at constant surface pressures of $\pi = 10$ mN/m

*uttam.basak@saha.ac.in
†alokmay.datta@saha.ac.in

to 40 mN/m (at 5 mN/m intervals) for C20 and C18, at π = 1 mN/m and from 5 mN/m to 35 mN/m at 5 mN/m intervals for C16, and at π = 1 mN/m, 2 mN/m, and from 5 mN/m to 25 mN/m at 5 mN/m intervals for C14. Data were collected at 10 °C, 15 °C, 20 °C, and 25 °C by maintaining subphase temperature using a Julabo recirculating cooler (FL300).

Brewster angle microscopy of monolayers was performed with an imaging ellipsometer (EP3, Accurion GmBH) in the BAM mode. Laser intensity was kept high to increase the contrast of the BAM image and thereby distinguish between monolayers and multilayers. The time for a monolayer to transform entirely into multilayers was obtained from a BAM movie filmed at 8 frames per second (fps) during monolayer relaxation via nucleation. To obtain the ellipsometry thickness map of C20 monolayers, all the films are deposited on a hydrophilic Si(100) substrate at different relaxation times at 25 mN/m 25 °C using the modified Langmuir-Schaefer technique [28–30]. Ellipsometric measurements were performed on the deposited samples using the imaging ellipsometer. For layers appreciably thinner than the wavelength of the probing light the Δ value is sensitive to the change in the layer thickness, while the Ψ value is hardly affected; we define the angles Ψ and Δ by the relation $r_p/r_s = \tan\Psi e^{\Delta}$ with $r_{p(s)}$ being the complex amplitude reflection coefficient for light polarized parallel (normal) to the reflection plane. We obtain the ellisometric angle Δ map for each sample. The optical modeling was performed with the software EP4 (Accurion) to obtain the thickness map of the sample. The details of imaging ellipsometry and modeling can be found in [31]. The optical functions of crystalline Si and SiO_2 are well known and implemented in the EP4 software. For arachidic acid, we use a single fixed value of the refractive index (n = 1.457) in all the thickness maps. Absorption by such a thin film is neglected (k = 0).

III. DESORPTION DYNAMICS

Figure 1(a) shows area fraction vs time (A_n-t) curves (symbols) for C14 monolayers at different π values on a pure aqueous subphase at 25 °C, as extracted from isotherms. The curve at a particular π was obtained by maintaining the monolayer at that π, measuring the monolayer area as a function of time (t), and normalizing the area values with the initial area. All the curves are fit very well by single-exponential decay functions (lines) showing that C14 undergoes DD dynamics and can be explained by a simple, semiempirical model of the desorption mechanism, which assumes that the desorption rate depends on the total number of surfactant molecules at the interface.

Let N be the total number of surfactant molecules in a monolayer of area A at any instant t. π is a function of the concentration of molecules at the interface ($\rho = \frac{N}{A}$).

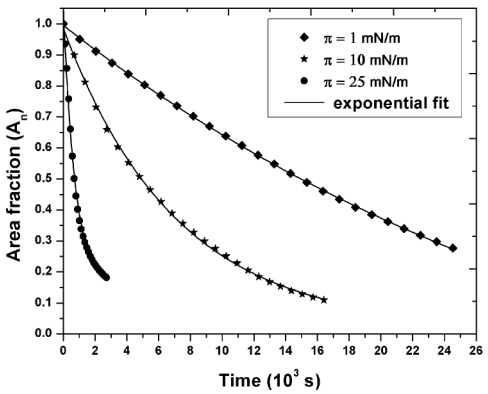

(a)

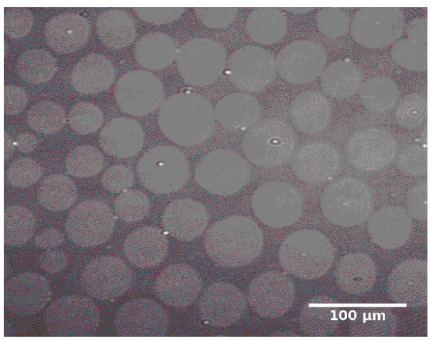

(b) time ∼ 1 min

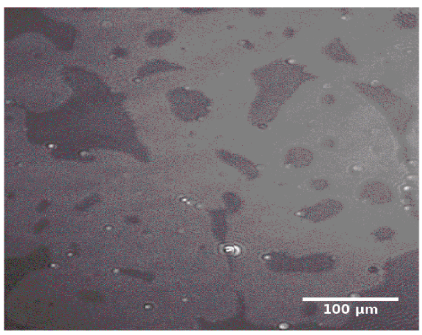

(c) time ∼ 40 min

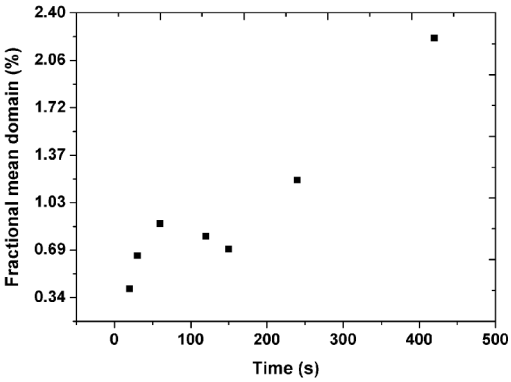

(d)

FIG. 1. (Color online) (a) Area fraction vs time (A_n-t) curves of myristic acid (C14) monolayer at different surface pressures (π), 25 °C, and on the pure aqueous subphase (ambient conditions), with corresponding exponential fits [lines, Eq. (2)]. See text for details. (b) and (c) Brewster angle microscope images of C14 at π = 20 mN/m and 25 °C. (d) Fractional mean domain area (i.e., mean domain area divided by the field of view) plot with time.

Hence, for a fixed π, ρ is a constant and $N = \rho A$. From our assumptions,

$$\left(\frac{\Delta N}{\Delta t}\right)_{\pi} = -kN, \tag{1}$$

leading to

$$A_n(t) = A_i e^{-kt}, \tag{2}$$

where k is a decay constant (its reciprocal is the time constant τ) which depends on ρ and temperature and A_i is the initial monolayer area fraction ($\sim$1.00). This model is consistent with the fact that desorption occurs at any nonzero pressure.

Figures 1(b) and 1(c) show the BAM images of C14 monolayers at $\pi = 20$ mN/m and 25 °C at different relaxation times. At high π different 2D domains of C14 are seen to coalesce but no multilayers are formed, as is clear from the constant contrast of the BAM images. This indicates dissolution of amphiphiles into the subphase and hence confirms a DD mechanism, consistent with the shorter chain length of C14. The contrast with this model of continuous loss of the monolayer at the macroscopic scale, i.e., from A_n-t curves, is brought out clearly in Fig. 1(d), which shows the growth of the mean 2D domain area with time, where the sizes of the 2D domains are obtained using ImageJ [32] software. The curve shows three regimes. Initially, up to $t \sim 60$ s, the mean area increases steadily, after which there is a drop until $\sim$150 s, and then again a steady rise until 10 min. After this the coalescence prevents measurement of the domain areas. The image remains unaltered on the average with the covered and uncovered areas about the same although their locations change. The image after 40 min [Fig. 1(c)] is a typical example of this situation. Correlating this curve with direct observation of the images, we suggest that the first regime is of growth of the individual 2D domains while the number of domains remains nearly constant, the second regime is of creation of new domains while the domain size remains almost unchanged, thereby effectively reducing the mean area, and the third regime is that of coalescence of these domains. The fact that the final BAM image remains qualitatively unchanged, with covered and uncovered areas changing places, over a long time shows that the processes of desorption and coalescence are active simultaneously.

IV. NUCLEATION DYNAMICS

The A_n-t (symbols) curves of C20 monolayers at different values of π in Fig. 2(a) at 25 °C show that the curves are sigmoidal, indicating ND dynamics for these molecules, as expected from their chain lengths. The monolayer instability increases with π, and at $\pi \leqslant 15$ mN/m the A_n-t curves are

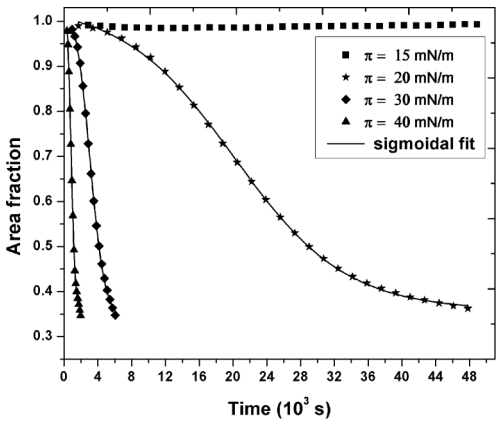

(a)

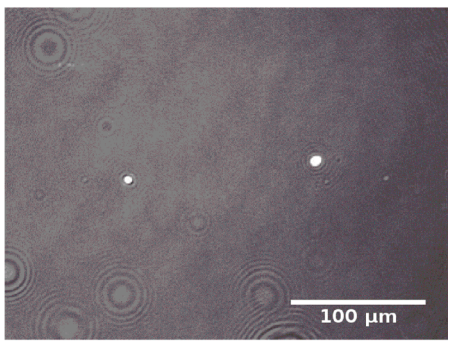

(b) time $\sim$ 3 min

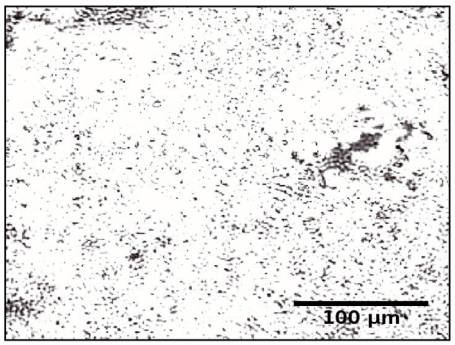

(c) time $\sim$ 95 min

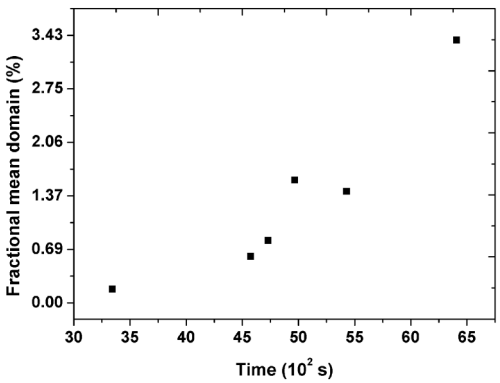

(d)

FIG. 2. (Color online) (a) A_n-t curves of arachidic acid (C20) monolayers at different surface pressures (π) and ambient conditions, with sigmoidal fits [lines, Eq. (3)]. See text for details. (b) and (c) Brewster angle microscope images of C20 at $\pi = 30$ mN/m and 25 °C. (d) Fractional mean domain area plot with time.

horizontal, indicating a stable monolayer (constant for $\geqslant$13 h). The behavior of C18 is very similar and hence is not shown.

We can model the nucleation mechanism as a self-limiting process. Let N_{2D} and N_{3D} be the total number of surfactant molecules in the 2D monolayer and in the 3D phase, respectively, at any instant t and N_0 ($=N_{2D}+N_{3D}$) is the total number of amphiphiles spread initially. Then for growth of the 3D phase

$$\left(\frac{\Delta N_{3D}}{\Delta t}\right) \propto N_{3D}\left(1-\frac{N_{3D}}{N_0}\right),$$

where the term linear in N_{3D} stands for the unimpeded 3D phase growth while the negative quadratic term in N_{3D} models the self-limiting due to depletion in N_{2D}. In terms of N_{2D} ($=N_0-N_{3D}$), we have for decay of the 2D phase

$$\left(\frac{\Delta N_{2D}}{\Delta t}\right) \propto -N_{2D}\left(1-\frac{N_{2D}}{N_0}\right).$$

For fixed π, ρ is a constant and $N_{2D_{(e)}}=\rho A$, where $N_{2D_{(e)}}$ includes the monolayer and also the base layer of the multilayers in contact with the water subphase. We assume that growth of multilayers stops only when the monolayer is totally depleted. Thus $N_{2D_{(e)}}$ can be considered to be N_{2D} [22]. Then we have

$$\left(\frac{\Delta A}{\Delta t}\right)_{\pi} \propto -A\left(1-\frac{A}{A_0}\right)$$

or

$$A_n(t) = A_f + \frac{A_i - A_f}{1+e^{k(t-t_0)}}, \tag{3}$$

where A_0, A_f, k, and t_0 are the initial monolayer area, the final area fraction ($\sim$0.2), the decay constant (measuring the steepness of the curves), and the inflection point (2D-3D coexistence time), respectively. This function has been used to fit the relaxation curves of nucleation in Fig. 2(a) (line).

Figures 2(b) and 2(c) are the BAM images of C20 monolayers at different times during relaxation at $\pi = 30$ mN/m and 25 °C. It is evident that these relaxations, unlike C14, correspond to the monolayer to multilayer transformation, i.e., nucleation, starting from multilayer centers shown as bright dots formed randomly over the entire monolayer, which grow and coalesce along with growth of new multilayer centers [Fig. 2(b)], until the entire monolayer is transformed into multilayers [Fig. 2(c)], confirming this to be a ND process. However, the time for monolayer to multilayer transformation is different for C20 and C18 monolayers at the same π. Comparison of BAM and isotherm data indicates a clear correlation between nucleation and sigmoidal decay, but it is to be noted that these sigmoidal profiles are observed only when the data are taken over a significantly long time and hence apparently they have not been observed before. Figure 2(d) shows the time variation of the mean area of 3D domains of the C20 monolayer as it relaxes at $\pi = 30$ mN/m and 25 °C. As in the case of DD dynamics, three regimes are present. Until $\sim$5000 s there is steady growth although the growth curve is concave, in contrast to the convex growth curve for 2D domains in DD dynamics. This is followed by a small region of near constant value of the mean area, and finally the area grows steadily again. However, unlike the 2D domains, there are almost no 3D domains in the beginning and hence in the first regime creation of nucleation centers is followed by domain growth and these processes take place together at the end of this regime. After this a short-lived regime of nucleation center creation and coalescence of 3D domains takes place that effectively lowers the mean area. Finally a coalescence-dominated regime comes into play until the domains cannot be distinguished and the whole field of view is covered [Fig. 2(c)].

BAM studies show that in-plane coalescence is the common and crucial process in both desorption and nucleation dynamics. The importance of 2D coalescence in ND dynamics has been shown through previous BAM studies [33] but there appears to be a dearth of data about its importance in DD dynamics. We suggest that these results point to the importance of the lipophilic force in monolayer dynamics on a long time scale.

V. CONTROL PARAMETERS

A. Surface pressure

The time constants ($\tau = k^{-1}$) of C14, C18, and C20 monolayers as functions of surface pressure at 25 °C are shown in Fig. 3(a). τ may be treated as a measure of stability

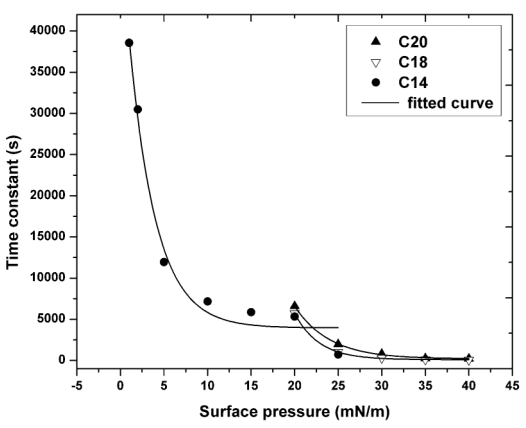

(a)

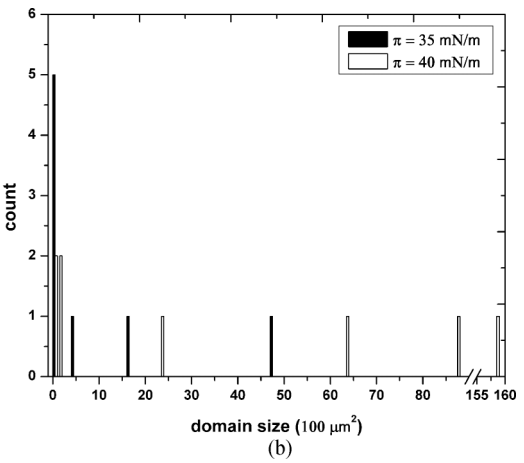

(b)

FIG. 3. (a) Time constants (τ), obtained by fitting A_n-t curves of C14 with Eq. (2) and those of C18 and C20 with Eq. (3), at different surface pressures and ambient conditions. (b) Distribution of 3D domains from BAM images of C20 at 35 and 40 mN/m and ambient conditions, after 15 min of relaxation.

of the monolayer against hydrophilic and lipophilic forces in desorption and nucleation, respectively, and is obtained from the fits of Eqs. (2) and (3) to the respective A_n-t curves. τ of C14 decreases exponentially with surface pressure. This enhanced desorption for larger 2D clusters suggests a correlated diffusion or superdiffusion, possibly due to the interaction between the "sheet" of dipoles (anions) from undissociated (dissociated) head groups and water [34].

Vysotsky *et al.* observed in their series of papers the spontaneous clustering of aliphatic amides for alkyl chain length higher than a threshold value, forming dimers and tetramers [35–37]. Goto *et al.* showed that during compression the hydrophilic groups are protruded in a new geometric configuration to form trilayer (or multilayer) structures [38]. Our results for the longer-chain acids are consistent with their studies. The stability of C20 and C18 decreases exponentially with surface pressure, probably because molecules can then come closer to form dimers, thereby turning hydrophobic and diffusing upwards to form multilayers.

Figure 3(b) shows the distribution of domain areas from BAM images of C20 monolayers at 35 and 40 mN/m, respectively, after 15 min of relaxation. The maximum domain area grows from ∼4800 to ∼16 000 μm^2. This increase in domain area indicates a 2D growth, and from direct observation of BAM movies, 2D coalescence is seen to take place in addition to 3D nucleation.

B. Temperature

The time constants of C14, C18, and C20 monolayers at $\pi = 20$ mN/m as functions of temperature are shown in Fig. 4(a). The stability of C14 remains constant up to 293 K and then falls down rapidly, which indicates the overcoming of the surface barrier due to tail-water hydrophobic repulsion. This gives a value of this barrier around 25 meV—a remarkably low value, again suggesting a correlation between the head groups and water that acts against the hydrophobic repulsion.

The stability of C20 and C18 decreases linearly with the temperature but this dependence is weak relative to that of C14 with temperature, as shown in Table I. The weak dependence of C20 monolayer dynamics on temperature can also be seen from BAM studies at 35 mN/m after 25 min of relaxation [Fig. 4(b)]. The number of domains within 0–1000 μm^2 remains very small, and the area of the largest domain increases from 1600 μm^2 at 15 °C to 5850 μm^2 at 25 °C. Again, this area increase shows a 2D growth, and direct visualization of the movies indicates 2D coalescence.

VI. CROSSOVER OF DYNAMICS

The relaxation curves of C16 at 25 °C are sigmoidal at higher surface pressures [Fig. 5(a)] but exponential at lower pressures [Fig. 5(b)], showing that a C16 monolayer, with tail length between those of C14 and C18, destabilizes via both ND and DD mechanisms. Above the critical surface (density) of 20 mN/m the enhanced lipophilic attraction makes nucleation dominant, leading to sigmoidal shape of the transformation curves. Below it the attraction drops and the dominant mechanism of destabilization starts to be desorption. Around 20 mN/m, the A_n-t curves are of a nature intermediate between the processes and the contribution of each is sensitive to changes in π.

These results are borne out by the BAM images of C16 during constant-pressure relaxation at high [30 mN/m, Fig. 5(c)] and low [1 mN/m, Fig. 5(d)] π. The C16 monolayer collapses completely at $\pi = 30$ mN/m via a 2D to 3D transition after 90 min, while no multilayer is formed even after 10 h at $\pi = 1$ mN/m and some material disappeared from the interface during the constant-pressure relaxation. This is the clearest evidence of the importance of tail length and lipophilic interactions.

VII. OUT-OF-PLANE GROWTH IN ARACHIDIC ACID MONOLAYERS

Out-of-plane ND dynamics away from the collapse pressure of the monolayer is another important aspect of the long-time-scale behavior. This requires the study of the height variation over a typical portion of the monolayer plane as a function of time. Height maps over a window of 337.00 × 813.35 μm^2 (370 × 893 pixels) were extracted from the Δ maps provided by IE for C20 monolayers at $\pi = 25$ mN/m

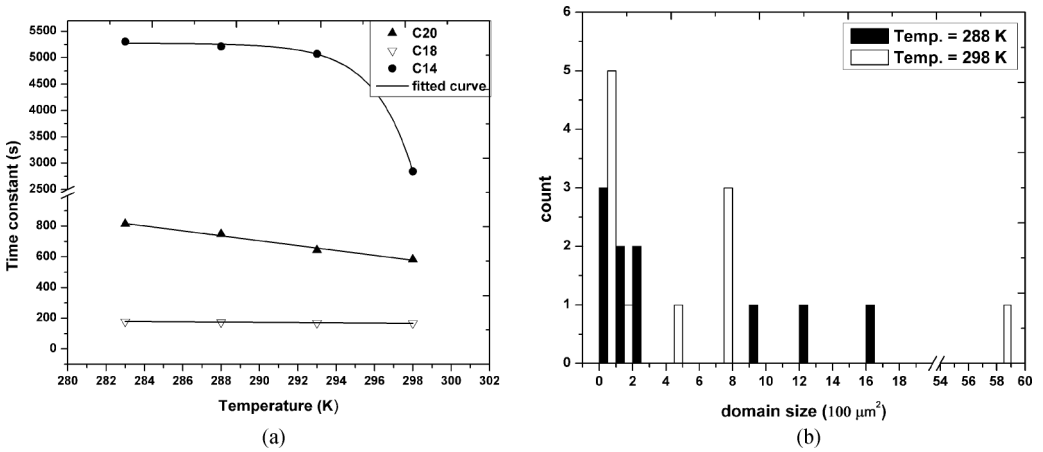

(a) (b)

FIG. 4. (a) τ, obtained by fitting A_n-t curves of C14 with Eq. (2) and those of C18 and C20 with Eq. (3), at different temperatures and 35 mN/m on pure water. (b) Distribution of 3D domains from BAM images of C20 at 288 and 298 K and the above conditions, after 25 min of relaxation.

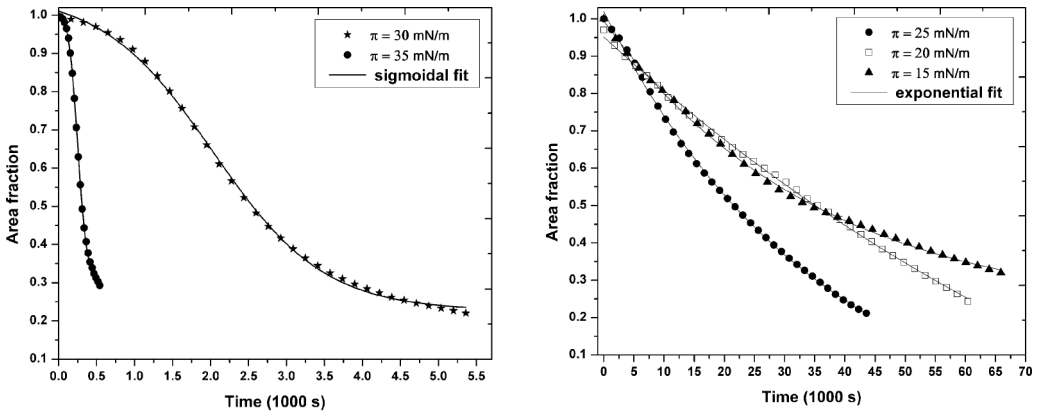

(a) (b)

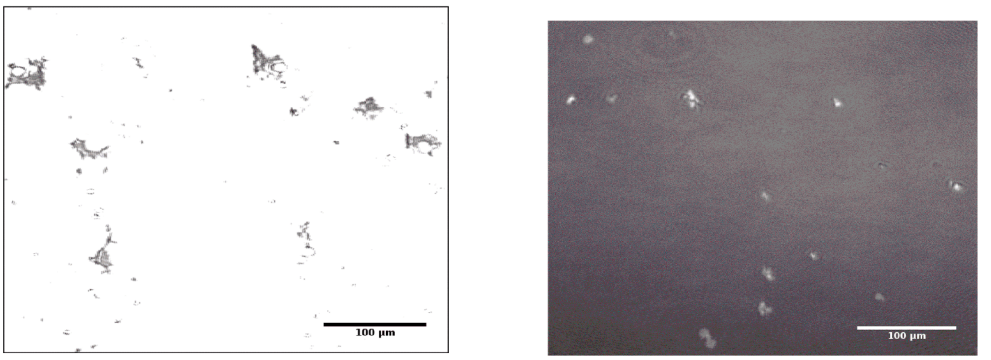

(c) time ∼ 90 min (d) time ∼ 10 h

FIG. 5. (Color online) A_n-t curves of palmitic acid (C16) monolayers at high and low π and ambient conditions, with (a) sigmoidal fits for high pressures and (b) exponential fits for low pressures. BAM images of a C16 monolayer at (c) $\pi = 30$ mN/m and (d) $\pi = 1$ mN/m for different collapse times.

and 25 °C, deposited by the MILS technique on hydrophilic Si(100), as described in Sec. II, at times of 30, 60, 90, 180, and 240 min and shown in Figs. 6(a), 6(c), 6(e), 6(g), and 6(i), respectively, in false color with corresponding typical line profiles shown in Figs. 6(b), 6(d), 6(f), 6(h), and 6(j). The thicker line in each of the latter represents an averaging over 100 adjacent points and gives the essential feature of the height variation. They depict a complex dynamics that merits description.

There are four major aspects of this dynamics—growth of a flat or smooth film, growth of multilayered islands, growth of multilayer ridges from coalescence of these islands, and evolution of "wavelike" features from coalescence of these ridges. The smooth film growth dominates until 60 min from the beginning and continues throughout, but from the film at 60 min islands appear on this smooth surface and increase in both height and numbers, until, from 180 min onwards, they cover almost the entire surface. Ridges are observed at 120 min and they also grow in height and number with time.

The nominal thickness of a C20 monolayer with untilted chains being ≈2.2 nm, we find that until 60 min there is a coexistence between a monolayer and a film of thickness between a bilayer and a trilayer, which, from free-energy considerations, we tentatively assign to a trilayer with the top layer having highly tilted chains. Until 30 min the monolayer is dominant while from 60 min this trilayer starts to dominate up to 180 min when a pentalayer (again with a tilted layer at the top) appears and grows in coverage in the background.

The average height of islands grows from ≈4 to 20 nm. At 90 min we find some island clusters of size 30 × 50 μm^2 but after that such isolated clusters are replaced by ridges spanning the field of view. The average height of the ridges grows from ≈6 to 10 nm and their average thickness grows from 80 to 250 μm from 120 to 240 min. They are found to grow roughly parallel to the trough barriers, i.e., perpendicular to the direction of shrinkage of the monolayer area. From 180 min onwards we see a new trend in the growth dynamics—the emergence of wavelike structures, most probably from the lateral coalescence of ridges. They become prominent in Fig. 6(i) and even more in the line profile of Fig. 6(i), i.e., at 240 min. The height of these waves can reach 25–30 nm while the "wavelength" is around 300 μm. Since the amplitude here is more than four orders of magnitude smaller than the wavelength, we propose that the in-plane agglomeration of molecules is much faster than their out-of-plane motion.

The square of the average height ($\langle h \rangle^2$) of the film is plotted with time in Fig. 7. The average height ($\langle h \rangle$) corresponds to the effective upward displacement of a molecule. From the plot it is clear that, after the first 2000 s (≈30 min) when it remains constant (monolayer), $\langle h \rangle$ varies linearly with $t^{1/2}$. This dependence of average height on time of growth bears a striking

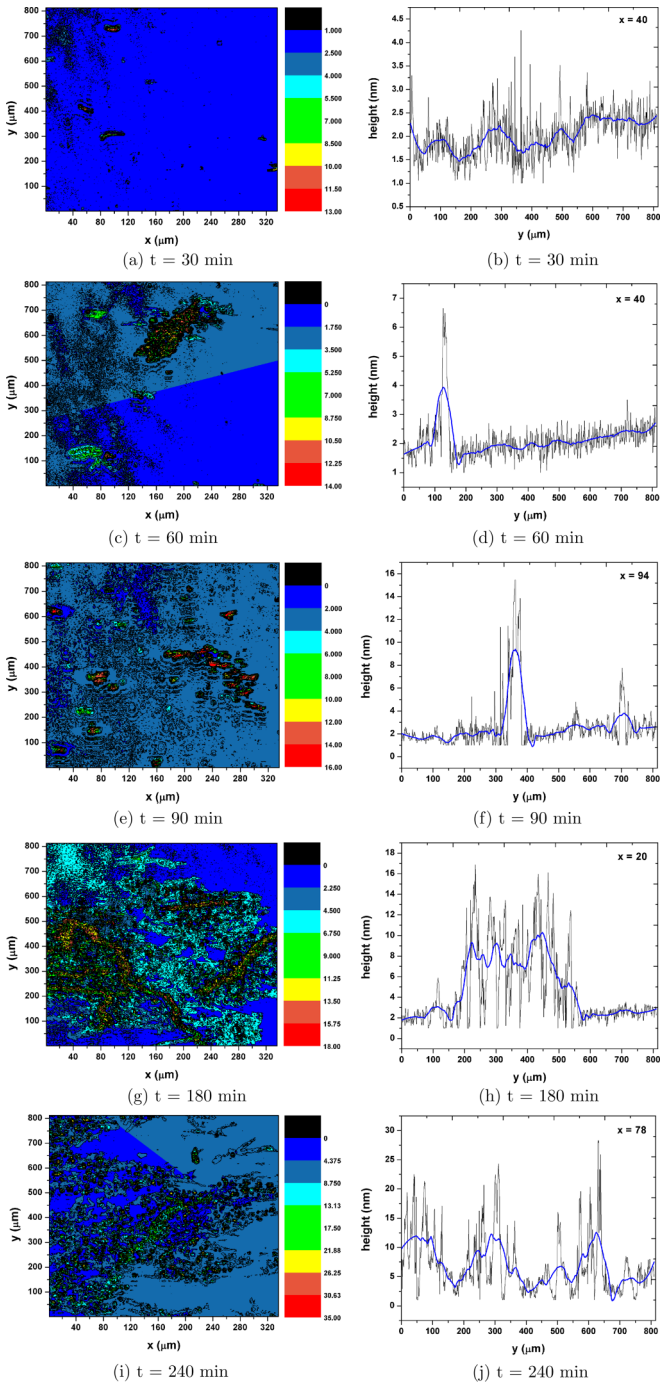

(a) t = 30 min (b) t = 30 min
(c) t = 60 min (d) t = 60 min
(e) t = 90 min (f) t = 90 min
(g) t = 180 min (h) t = 180 min
(i) t = 240 min (j) t = 240 min

FIG. 6. (Color online) False color height contour plots obtained from imaging ellipsometry of arachidic acid (C20) film on water transferred horizontally onto hydrophilic Si(100) substrates after the corresponding times after monolayer formation with the color scale shown next to the plots. A typical line profile from each contour plot follows the plot. The blue line is an average over 100 adjacent points.

similarity with a situation when molecules undergo upward diffusion through the air/monolayer interface, with the slope of the plot, calculated to be 0.0033 nm^2/s, giving the value of the upward diffusivity of the amphiphile. However, in the absence of any direct evidence of diffusive dynamics, we refrain from proposing such behavior as an explanation of the results.

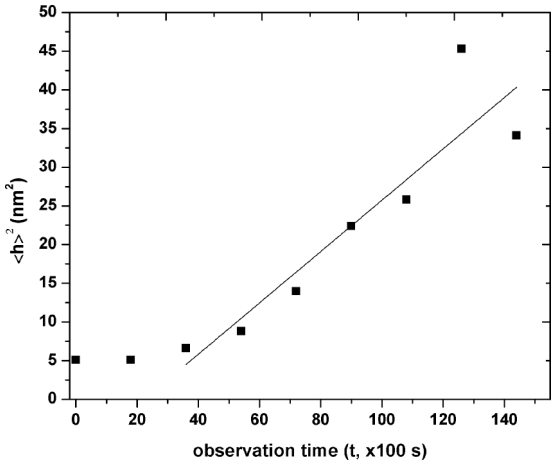

FIG. 7. Square of average height ($\langle h \rangle$,nm) of C20 films, transferred onto hydrophilic Si(100) and measured from imaging ellipsometry, plotted against observation time (t,s). The linear fit of the data is taken after 2000 s.

Similar growth dynamics has been observed for monolayers of cobalt stearate, a two-tailed amphiphilic, at constant-pressure collapse [22]. The mechanism for the 2D to 3D transition is again diffusion as it was in that case. However, there are significant differences between the systems and the results of our studies and we shall enumerate them. (1) One major difference is, of course, that we are studying a monolayer at far below the collapse pressure of 42 mN/m, whereas for the stearate monolayer the surface pressure went up to as high as 61 mN/m. Hence we are here in the stable zone of the monolayer, in contrast to the completely unstable, collapsing monolayer in that other case. (2) The other difference is that our system is a monolayer of single-tailed amphiphiles while the stearate was, as said, a two-tailed amphiphile. We would expect a completely different behavior in our system, and the fact that the basic dynamics occurs through the formation of multilayers—both films and islands—in fatty acids and stearate indicates an underlying universality in these 2D to 3D transitions. We find the growth to be in steps of bilayers and thus, along with the fact that upward transfer through the monolayer and the subsequent multilayers can occur only if the hydrophilic nature of the carboxylic head groups (due to the dipole moment) is suppressed, leads to the conclusion that adjacent fatty-acid molecules in the monolayer are dimerized at the head groups through lipophilic attraction. Thus the lipophilic force again plays a pivotal role in the 2D to 3D transition, and the dimer is transferred upwards with its two tails disposed symmetrically about the dimerized head groups. This dimerization is, as discussed earlier, consistent with previous results obtained by Vysotsky *et al.* [36] and Goto *et al.* [38]. Although both have the essential characteristics of Stranski-Krastanov growth, while the upward drift of molecules is present throughout the growth in this case of arachidic acid away from collapse, it could not be detected clearly in the collapse of cobalt stearate. However, the most important difference is the emergence of the set of wavelike structures from the in-plane coalescence of ridges on the film surface. The in-plane coalescence, which plays the dominant

role in all of out-of-plane growth, is further evidence of the importance of the lipophilic force.

VIII. CONCLUSION

Mesoscopic (Brewster angle microscopy and imaging ellipsometry) and macroscopic (surface pressure–area or π-A isotherm) methods have been used to understand the details of long-term destabilization dynamics in Langmuir monolayers. We have used the isotherms to extract the monolayer area fraction versus time (A_n-t) curves and these form the bases of our macroscopic studies of the destabilization dynamics, while the BAM images form the mesoscopic bases. We have found that the results obtained from the two techniques bring out two aspects of the monolayer dynamics. While the isotherm studies show the desorption-dominated destabilization to be given by an exponentially decaying A_n-t curve pointing to a single, continuous loss of the monolayer by dissolution, the BAM studies reveal a two-dimensional coalescence taking place simultaneously with the loss. On the other hand, a nucleation-dominated destabilization emerges as a self-limiting process at both length scales. In both desorption and nucleation the initial step is a two-dimensional coalescence at the mesoscopic scale. Instabilities in monolayer are suggested to originate from packing defects at domain edges due to conflicting molecular orientations [39] or height differences at the boundary between 2D phases [40], but our BAM studies show that 3D nucleation occurs in C20 and C18 monolayers with one single phase, consistent with Ybert *et al.* [25].

From A_n-t curves we have extracted the decay time constant (τ) as a parameter to quantify the stability in Langmuir monolayers and looked at the effects of π and temperature on τ. This analysis shows that (1) both desorption and nucleation are enhanced at higher surface pressures; for nucleation there exists a threshold pressure below which nucleation is absent whereas no threshold pressure is found for desorption; and (2) both the destabilization mechanisms are enhanced with temperature. However, we have found that the most important factor regarding destabilization is the tail length of molecules. This molecular parameter not only decides the time constant of the 2D-3D transformation on the external parameters but also causes a crossover from nucleation to desorption as the tail length is decreased below a certain value with the same head group. Imaging ellipsometry has been used to extract the height contour maps of the different stages of dynamics of out-of-plane growth of a C20 monolayer, after horizontal transfer of the film onto Si(100) surface at these stages. It is seen that monolayer growth is followed successively by trilayer and multilayer islands, ridges through island coalescence, and shallow wavelike structures through ridge coalescence, having an essential resemblance with Stranski-Krastanov growth but with specific characteristics. While the molecules are transferred to the upper layers by diffusion, in-plane coalescence mediated by lipophilic attraction plays the crucial role in the evolution of these structure. Again, this attraction dimerizes the adjacent fatty-acid molecules in the monolayer to initiate diffusion. All these results have led us to conclude that the lipophilic attraction between the tails of the fatty-acid monolayer is the driving or dominant force in the long-term dynamics of fatty-acid Langmuir monolayers.

ACKNOWLEDGMENT

U.K.B. thanks the University Grants Commission (UGC) (India) for their financial support.

[1] G. Brezesinski and H. Möhwald, Adv. Colloid Interface Sci. **100-102**, 563 (2003).
[2] G. Alegria and P. L. Dutton, Biochim. Biophys. Acta, Bioenerg. **1057**, 239 (1991).
[3] G. Thakur, M. Micic, and R. M. Leblanc, Colloids Surf., B **74**, 436 (2009).
[4] Y. Okahata, T. Tsuruta, K. Ijiro, and K. Ariga, Thin Solid Films **180**, 65 (1989).
[5] C. Nunes, G. Brezesinski, C. Pereira-Leite, J. L. F. C. Lima, S. Reis, and M. Lúcio, Langmuir **27**, 10847 (2011).
[6] A. A. Torrano, Ângela S. Pereira, O. N. O., Jr., and A. Barros-Timmons, Colloids Surf., B **108**, 120 (2013).
[7] W. Schulte, M. Orlof, I. Brand, B. Korchowiec, and E. Rogalska, Colloids Surf., B **116**, 389 (2014).
[8] A. Serro, R. Galante, A. Kozica, P. Paradiso, A. G. da Silva, K. Luzyanin, A. Fernandes, and B. Saramago, Colloids Surf., B **116**, 63 (2014).
[9] C. B. Tovani, J. F. V. de Souza, T. de Souza Cavallini, G. J.-F. Demets, A. Ito, M. B. Barioni, W. M. Pazin, and M. E. D. Zaniquelli, Colloids Surf., B **111**, 398 (2013).
[10] G. J. Ashwell, J. Mater. Chem. **9**, 1991 (1999).
[11] V. Krstic, G. S. Duesberg, J. Muster, M. Burghard, and S. Roth, Chem. Mater. **10**, 2338 (1998).
[12] G. Roberts, Sens. Actuators **4**, 131 (1983).
[13] M. Sugi, J. Mol. Electron. **1**, 3 (1985).
[14] B. Tieke, Adv. Mater. **2**, 222 (1990).
[15] P. Vincett and G. Roberts, Thin Solid Films **68**, 135 (1980).
[16] M. Iwahashi, N. Maehara, Y. Kaneko, T. Seimiya, S. Middleton, N. Pallas, and B. Pethica, J. Chem. Soc., Faraday Trans. 1 **81**, 973 (1985).
[17] S. Siegel, D. Hönig, D. Vollhardt, and D. Moebius, J. Phys. Chem. **96**, 8157 (1992).
[18] A. Angelova, D. Vollhardt, and R. Ionov, J. Phys. Chem. **100**, 10710 (1996).
[19] R. D. Smith and J. C. Berg, J. Colloid Interface Sci. **74**, 273 (1980).
[20] H. Diamant, T. Witten, A. Gopal, and K. Lee, EPL (Europhys. Lett.) **52**, 171 (2000).
[21] V. M. Kaganer, H. Möhwald, and P. Dutta, Rev. Mod. Phys. **71**, 779 (1999).
[22] S. Kundu, A. Datta, and S. Hazra, Phys. Rev. E **73**, 051608 (2006).
[23] S. Kundu, A. Datta, and S. Hazra, Langmuir **21**, 5894 (2005).
[24] K. Lee, Annu. Rev. Phys. Chem. **59**, 771 (2008).

[25] C. Ybert, W. Lu, G. Möller, and C. M. Knobler, J. Phys. Chem. B **106**, 2004 (2002).
[26] S. Baoukina, L. Monticelli, H. J. Risselada, S. J. Marrink, and D. P. Tieleman, Proc. Natl. Acad. Sci. **105**, 10803 (2008).
[27] K. Birdi and D. Vu, Langmuir **10**, 623 (1994).
[28] T. Kato, N. Matsumoto, M. Kawano, N. Suzuki, T. Araki, and K. Iriyama, Thin Solid Films **242**, 223 (1994).
[29] M. M. Lipp, K. Y. C. Lee, D. Y. Takamoto, J. A. Zasadzinski, and A. J. Waring, Phys. Rev. Lett. **81**, 1650 (1998).
[30] S. Mukherjee, A. Datta, A. Giglia, N. Mahne, and S. Nannarone, Langmuir **25**, 3519 (2009).
[31] M. M. B. Nielsen and A. C. Simonsen, Langmuir **29**, 1525 (2013).
[32] J. Schindelin, I. Arganda-Carreras, E. Frise, V. Kaynig, M. Longair, T. Pietzsch, S. Preibisch, C. Rueden, S. Saalfeld, B. Schmid *et al.*, Nat. Methods **9**, 676 (2012).
[33] D. Vollhardt, Adv. Colloid Interface Sci. **123-126**, 173 (2006), special issue in honor of Dr. K. L. Mittal.
[34] W. C. Duncan-Hewitt, Langmuir **7**, 1229 (1991).
[35] Y. B. Vysotsky, E. S. Fomina, E. A. Belyaeva, E. V. Aksenenko, V. B. Fainerman, D. Vollhardt, and R. Miller, J. Phys. Chem. B **115**, 2264 (2011).
[36] Y. B. Vysotsky, E. S. Fomina, E. A. Belyaeva, D. Vollhardt, V. B. Fainerman, and R. Miller, J. Phys. Chem. C **116**, 26358 (2012).
[37] Y. B. Vysotsky, E. S. Fomina, V. B. Fainerman, D. Vollhardt, and R. Miller, Phys. Chem. Chem. Phys. **15**, 11623 (2013).
[38] T. E. Goto and L. Caseli, Langmuir **29**, 9063 (2013).
[39] W. R. Schief, L. Touryan, S. B. Hall, and V. Vogel, J. Phys. Chem. B **104**, 7388 (2000).
[40] H. Diamant, T. A. Witten, C. Ege, A. Gopal, and K. Y. C. Lee, Phys. Rev. E **63**, 061602 (2001).